High Performance Yacht Design HPYD8 Conference, 21-22 March 2024, Auckland, New Zealand.

CFD Study on the Different Stratifications of the Atmospheric Boundary Layer and their Effect on the Performance of Wind Propelled Ships

Chiara Wielgosz
RISE, SSPA Maritime Centre, Sweden; KTH Royal Institute of Technology, Sweden, chiara.wielgosz@ri.se

Laura Marimon Giovannetti
RISE, SSPA Maritime Centre, Sweden.

Sofia Werner
RISE, SSPA Maritime Centre, Sweden.

Jakob Kuttenkeuler
KTH Royal Institute of Technology, Sweden.

Abstract.
CFD simulations to predict forces from a Wind Propulsion Unit (WPU) on a ship hull are carried out to better understand the forces dependency on wind speed and angle. Three different Atmospheric Boundary Layer (ABL) stratifications, nominally unstable, neutral and stable, are studied in a Computational Fluid Dynamic (CFD) environment to better understand how to reproduce these velocity profiles in CFD and how much is their impact on the performance of a ship equipped with a Flettner rotor. A series of 2D and 3D simulations with an empty domain are run to tune some numerical settings for a correct representation of the ABL. To study the challenging aspects of reproducing an ABL in CFD, it is suggested to tune the parameters in an empty 3D domain. Simulations with a simplified hull and a Fletter rotor are run. The three different ABL profiles are tested for four different wind angles, producing an overview of the dependency of rotor and ship performance on wind speed profiles, wind angles and hull interaction. A clear impact of the wind angle and wind profiles is visible on the rotor lift and drag coefficient, while in terms of ship performance, described by the ratio of the thrust and side force coefficients, the impact is limited.

Keywords: wind propulsion; atmospheric boundary layer; CFD; Flettner rotor, hull interaction.

NOMENCLATURE

AR	Aspect ratio [-]
B	Breadth of the ship [m]
C_D	Drag coefficient [-]
C_L	Lift coefficient [-]
C_p	Pressure coefficient [-]
C_S	Side force coefficient [-]
C_T	Thrust coefficient [-]
C_μ	Turbulence model coefficient [-]
D	Flettner rotor diameter [m]
D_{ep}	Endplate diameter [m]
f	Freeboard of the ship [m]
k	Turbulence kinetic energy [J kg^{-1}]
L	Length of the ship [m]
r	Sand-grain roughness [m]
rpm	Rotation per minute [deg s^{-1}]

S	Surface area of the rotor and endplate [m^2]
SR	Spin ratio [-]
t	Time-step [s]
t_{ep}	Endplate thickness [m]
TI	Turbulence intensity [-]
TI_{ref}	Reference turbulence intensity [-]
u_x	Velocity in the x-direction [m s^{-1}]
U_{rh}	Velocity at mid-height of the rotor [m s^{-1}]
$u(z)$	ABL velocity profile [m s^{-1}]
U_{ref}	Reference velocity [m s^{-1}]
y^+	Dimensionless wall distance [-]
z	Vertical position [m]
z_{ref}	Reference height [m]
z_0	Atmospheric height [m]

α	Hellmann exponent [-]
β^*	Alternative symbol for C_μ [-]
δ	Prism layer total thickness [m]
Δp	Differential pressure [Pa]
ε	Turbulence dissipation rate [m^2 s^{-3}]
μ	Fluid dynamic viscosity [Pa s]
μ_t	Turbulence eddy viscosity [Pa s]
ρ	Fluid density [kg m^{-3}]
ω	Specific turbulence dissipation rate [s^{-1}]

ABL	Atmospheric Boundary Layer
AIJ	Architectural Institute of Japan
AWA	Apparent Wind Angle
CFD	Computational Fluid Dynamics
IMO	International Maritime Organization
ITTC	International Towing Tank Conference
KVLCC	KRISO Very Large Crude Carrier
NPD	Norwegian Petroleum Directorate
RANS	Reynolds-Averaged Navier-Stokes
SST	Shear-Stress Transport
uRANS	Unsteady Reynolds-Averaged Navier-Stokes
WPU	Wind Propulsion Unit

1. INTRODUCTION

In the increasing need to find renewable resources to decrease the human footprint on the environment and the approaching of 2030, when new-built and existing ships carbon intensity must be lowered by at least 40% as specified by the International Maritime Organization (IMO) regulations, the shipping industry has shown its interest in wind energy.
An important aspect for the correct development of these new technologies is the wind itself. This importance comes from the need of a correct prediction of the forces generated by these technologies, required for the design and fuel saving expectations, to take correct investment decisions. On the earth, as well as on the oceans, an Atmospheric Boundary Layer (ABL) is present in the troposphere, which height can vary between 100 and 3000 m from the ground, affecting the lowest part of the atmosphere. This boundary layer can have three different stratifications: nominally neutral, stable, and unstable. They are characterized by different thermal stratifications that affect the vertical variation in wind velocity: a neutral stratification has an adiabatic temperature gradient; a stable one has a vertical temperature gradient lower than the adiabatic case, causing the wind velocity to increase faster with increasing altitude; in an unstable case, the temperature gradient, being higher that the adiabatic one, causes a slower increase in wind velocity with increasing altitudes. On the open water, the transition between different stratifications s observable throughout a year, in spring a tendency to stable stratification is present, while in late autumn the tendency is towards unstable layering (Kaltschmitt et al., 2007).
Wind powered ships will sail throughout the year and will encounter all three different stratifications of the boundary layer. In the wind propulsion research field, experiments in wind tunnels and numerical simulations, only utilize a unform profile or a neutral stratification of the ABL to describe the wind velocity. So far, it has not been studied to what extent the type of ABL stratification affects the performance of the Wind Propulsion Unit (WPU), nor the interaction of the superstructures with such flows.
The present study will try to answer these questions via Computational Fluid Dynamics (CFD) simulations. The study case is the simplified hull of the KVLCC2 tanker equipped with a Flettner rotor. Four different wind angles are tested, with values of the Apparent Wind Angles (AWA) equal to 30, 45, 60 and 90 degrees. The wind profile is described as suggested by the International Towing Tank Conference (ITTC): a semi-empirical power law expression with the exponent (Hellmann exponent) representing the stratification of the boundary layer. Three different exponents, representing the three different stratifications are adopted: for the neutral case the Hellmann exponent will be set to 1/9 (as suggested by ITTC 2022), for the unstable case the empirical Hellmann exponent computed from wind measurements at sea is used (Dhomé et al., 2023 under review), while for the stable case an approximated value found in literature is chosen (Kaltschmitt et al., 2007).

2. SETUP OF THE ABL PROFILES

2.1 Wind Description

The Atmospheric Boundary Layer is the realistic description of the wind present on the Earth and can be generically described by a log-law or a power-law. To correctly model the ABL in CFD simulations, additionally to the ABL velocity profile, it is important to prescribe profiles for the turbulence quantities (Richards and Norris, 2011). In function of the engineering application, it is possible to find different ABL and turbulence quantities formulations. In the offshore industry, the most used wind profile is the Norwegian Petroleum Directorate (NPD) wind model, described by a logarithmic law (Kim et al. 2018). In the field of wind turbines, as found in RahnamayBahambary and Fleck (2022), it is possible to find both descriptions, the log-law description, as given by Richards and Hoxey (1993), and the power-law description; in Tian et al. (2018) different ABL formulations are compared and in Tian et al. (2021) the power-law description is preferred for their simulations. In wind propulsion, we can find both formulations, a log-law description is present in Viola et al, (2015) and Bataille et al. (2023); while in Garenaux et al. (2020) and Garenaux and Schot (2021), as well as the 2022 International Towing Tank Conference, the power-law profile is applied.

In this paper, the power-law description in Eq. 1 is adopted, with the semi-empirical turbulence profiles in Eqs. 2-5 developed by the Architectural Institute of Japan (Tian et al. 2020):

$$u(z) = U_{ref}\left(\frac{z}{z_{ref}}\right)^{\alpha} \tag{1}$$

$$TI(z) = TI_{ref}\left(\frac{z}{z_{ref}}\right)^{-\alpha-0.05} \tag{2}$$

$$k(z) = \frac{dimension}{2}\left(u(z)TI(z)\right)^2 \tag{3}$$

$$\varepsilon(z) = {C_\mu}^{1/2}k(z)\frac{U_{ref}}{z_{ref}}\alpha\left(\frac{z}{z_{ref}}\right)^{\alpha-1} \tag{4}$$

$$\omega(z) = {C_\mu}^{-1/2}\frac{U_{ref}}{z_{ref}}\alpha\left(\frac{z}{z_{ref}}\right)^{\alpha-1} \tag{5}$$

where U_{ref} is the reference speed at height z_{ref}, z is the local height, α is the Hellmann exponent, $TI(z)$ is the vertical profile for turbulence intensity, TI_{ref} is the turbulence intensity level at z_{ref}, $k(z)$ is the vertical profile for turbulence kinetic energy, valid if isotropic turbulence is assumed, $dimension$ is equal to the dimensionality of your domain, e.g. if the simulation is in 2D it is equal to two while if the simulation is in 3D it is equal to three, $\varepsilon(z)$ is the vertical profile for the turbulence dissipation rate, C_μ is a coefficient present in the turbulence model and $\omega(z)$ is the vertical profile for specific dissipation rate of turbulence. To describe the different ABL stratifications, three different values of α are adopted as showed in Table 1 and the three different profiles are depicted in Figure 1.

Table 1. Values adopted for α to describe different ABL stratifications.

ABL stratification	α [-]	U_{rh} [m/s]	Reference
Unstable	0.039	10.5	Dhomé et al. (2023) under review
Neutral	1/9=0.11	11.5	ITTC (2022)
Stable	0.27	14.0	Kaltschmitt et al. (2007)

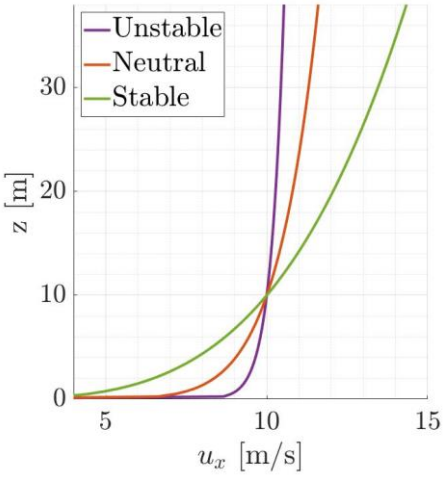

Figure 1. Representation of the three different ABL profiles used.

2.2 Empty Domain Simulations

A series of simulations with a 2D empty domain were carried out to setup the numerical environment to reproduce the three different atmospheric boundary layer profiles. The 2D rectangular empty domain has a length of 5000 meters and a height of 960 meters with the following boundary conditions: inlet velocity at the inlet and the top of the domain, pressure outlet at the outlet and no-slip wall at the bottom. The steady Reynolds-Averaged Navier-Stokes (RANS) equations are solved with the commercial code Star CCM+ 2206 (17.04.007). The equations are solved using a finite volume discretization with a collocated variable arrangement and a pressure-based approach. The coupling between momentum and continuity equations is achieved via the SIMPLE algorithm. The k-ω Shear-Stress Transport (SST) turbulence model is used. Convection and diffusivity schemes are second-order accurate for all the transport equations. The Newtonian fluid simulated is air at 15 degrees Celsius, with corresponding density ρ = 1.225 kg m^{-3} and dynamic viscosity μ = 1.802 x 10^{-5} kg m^{-1} s^{-1}. The mesh is composed by 16675 hexahedral cells. The prism layer total thickness δ is equal to 38 meters divided in 30 layers, achieving a y^+ value greater than 30.

For all the simulations presented in this paper, the following values to describe the ABL were used; the reference height z_{ref} is set to 10 m, the reference speed U_{ref} to 10 m s^{-1} and a reference turbulence intensity TI_{ref} equal to 10% was assumed, since common value found at open seas. For what concerns the turbulence coefficient C_μ, present in the k-ω SST turbulence model as β^* and the turbulence quantities profiles (Eqs. 4-5), three different values were tested: the default value equal to 0.09 (Menter 1994), the value suggested for wind engineering applications of 0.03 (Tian et al. 2018) and an even lower value equal to 0.013 found in Richards and Hoxey (1993). Additionally, different trials were done to tune the roughness of the bottom wall boundary to preserve the prescribed inlet profiles throughout the domain. In Star-CCM+ the roughness is described with the sand-grain roughness variable r; its value is obtaind by multiplying the atmospheric roughness z_0, equal to 0.001 m for rough seas, by a constant, namely a roughness multiplier. Another value that has influence on the simulation of the ABL is a variable in Star-CCM+ called the k-ω turbulent viscosity maximum ratio. The default value equal to 10^5 has been changed to 10^{10} in some cases, as suggested by best practice. After several combinations of these different values, the settings in Table 2 were found the most appropriate to reproduce the three different stratifications of the atmospheric boundary layer.

Table 2. Tuned settings to describe the three different stratifications of the atmospheric boundary layer.

ABL stratification	C_μ	Max μ_t/μ	Bottom surface	Roughness multiplier
Unstable	0.013	10^{10}	Smooth	-
Neutral	0.013	10^{10}	Rough	5
Stable	0.013	10^5	Rough	150

After the 2D empty domain simulations, to check the effect of three-dimensionality on the turbulence quantities, each profile was simulated in a 3D rectangular prism empty domain with the same general dimensions and boundaries of the domain with the simplified hull and rotor; the length of the domain is $8L$, the width is $7L$ and the height is $3.5L$, with L equal to 317.48 meters. At the inlet, sides and top of the domain, a velocity inlet is prescribed with the ABL profile (Eq. 1) and the turbulence profiles in Eqs. 3,5. The outlet is set as a pressure outlet and the bottom of the domain as a no-slip wall with and without roughness in function of the kind of ABL (see Table 2). The same numerical settings as for the 2D domain are used, while the total mesh density is of circa 1M hexahedral cells. The prism layer mesh has a total thickness δ equal to 33 meters with 24 prism layers and a y^+ value greater than 30. The height of the near wall cell is kept constant between the 2D and 3D simulations.

The profiles of the velocity in x-direction u_x, turbulence kinetic energy k and specific turbulence dissipation rate ω are presented for the three atmospheric boundary layers at different locations streamwise for the 3D simulations in Figures 2-4. For all three cases there is an under-production of turbulence kinetic energy close to the bottom of the domain that remains with height in the unstable case but transforms to over-production in the stable stratification. For what concerns the x-velocity profile, at the reference height z_{ref} of 10 meters, the unstable case has a difference between the velocity profile at the inlet and the outlet equal to 1.3%; for the neutral stratification this difference increases to 2.7% while for the stable case to 3.7%. In all three cases, this difference continues decreasing with height; while the opposite behaviour is observable for z-values close to the bottom, with a maximum value for the unstable case equal to 6.4%, for the neutral case to 8.2 % and for the stable case to 73%. Nevertheless, the results lead to the conclusion that the ABL is well-preserved throughout the domain.

Clearly, the stable stratification is the worst represented of the three, but these high differences are present in the lowest heights of the domain, and their impacts on the rotor performance are assumed marginal. The origin of the ship coordinate system and the rotational axis of the rotor coincide with the origin of the computational domain. The base of rotor is found 20 meters above the origin and the difference between the prescribed velocity profile and the velocity profile at this location is of 0.6% for the unstable ABL, -0.03% for the neutral one and 1.1% for the stable stratification.

The main difference observed between the 2D and 3D simulations is the higher levels of turbulence kinetic energy k close to the wall, causing an increase in speed at the lower heights. If possible, it is suggested to tune the ABL directly in a three-dimensional empty domain.

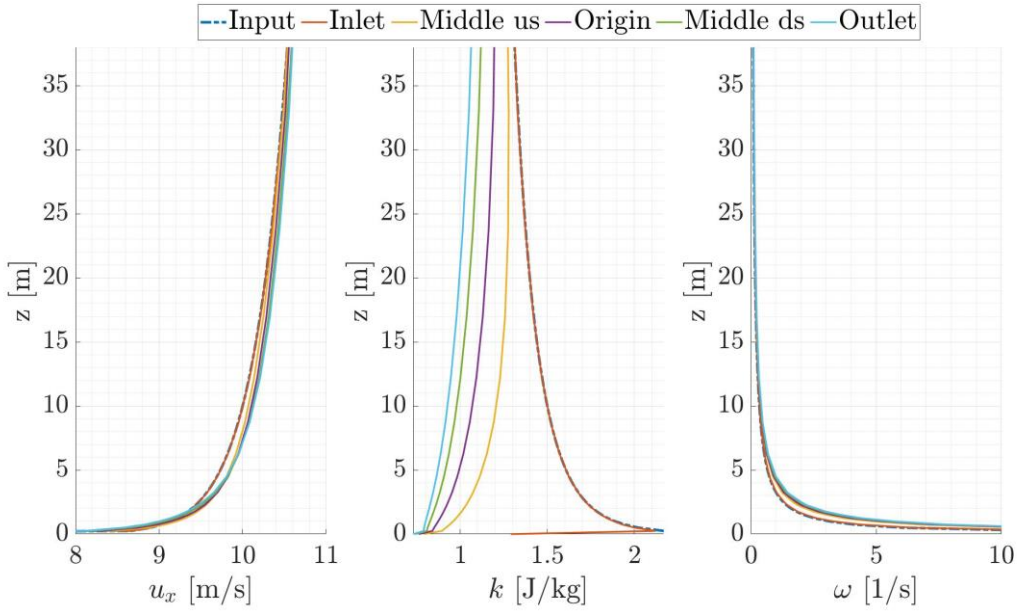

Figure 2. Unstable ABL: velocity in x-direction (left), turbulence kinetic energy k (center) and specific turbulence dissipation rate ω (right) profiles streamwise from the inlet to the outlet of the domain. Middle us stands for Middle upstream, x-location half way between the inlet and the origin of the domain; while Middle ds stands for Middle downstream, x-location half way between the origin and the outlet of the domain.

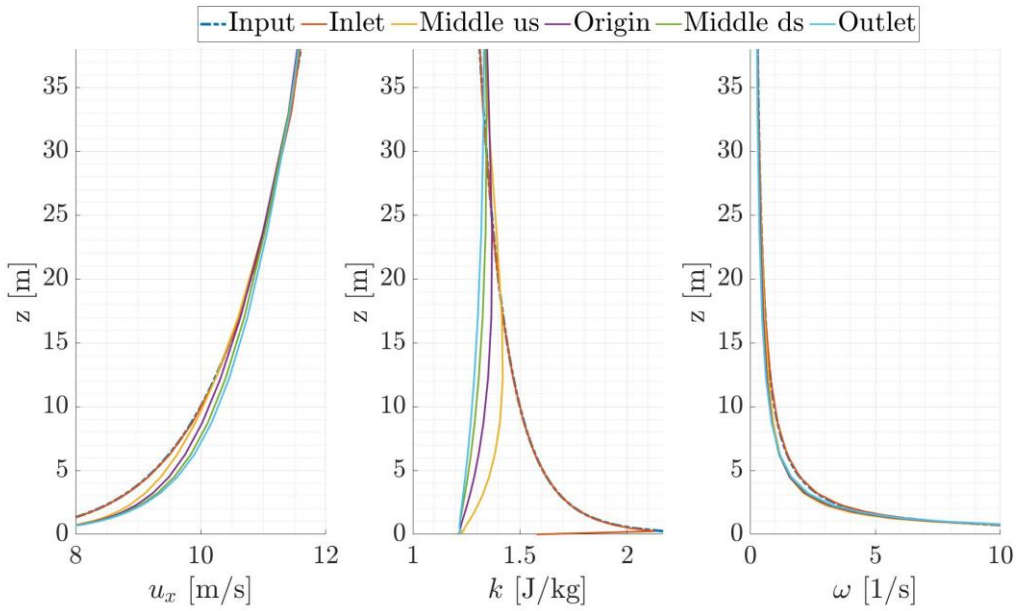

Figure 3. Neutral ABL: velocity in x-direction (left), turbulence kinetic energy k (center) and specific turbulence dissipation rate ω (right) profiles streamwise from the inlet to the outlet of the domain. Middle us stands for Middle upstream, x-location half way between the inlet and the origin of the domain; while Middle ds stands for Middle downstream, x-location half way between the origin and the outlet of the domain.

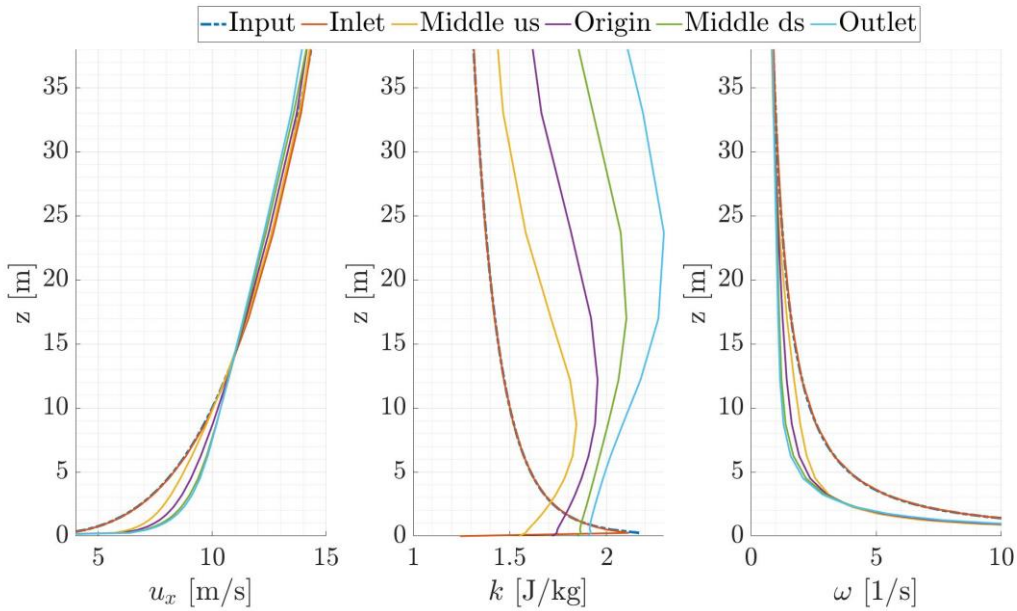

Figure 4. Stable ABL: velocity in x-direction (left), turbulence kinetic energy k (center) and specific turbulence dissipation rate ω (right) profiles streamwise from the inlet to the outlet of the domain. Middle us stands for Middle upstream, x-location half way between the inlet and the origin of the domain; while Middle ds stands for Middle downstream, x-location half way between the origin and the outlet of the domain.

3. FLETTNER ROTOR AND SIMPLIFIED HULL SIMULATIONS

3.1 CFD Setup

A simplified case is studied to achieve general preliminary results of the influence of the hull on the performance of a Flettner rotor with different atmospheric boundary layer stratifications and wind angles. The well-known KVLCC2 (KRISO Very Large Crude Carrier) ship is represented by a box with the general dimensions of the tanker in ballast conditions: the ship has length L equal to 317.48 m, breadth B of 5 m, freeboard f of 20 meters and ship speed equal to zero. A generic Flettner rotor with Aspect Ratio AR equal to 6 and diameter D of 5 meters, with an endplate of diameter D_{ep} equal to 10 m and of thickness t_{ep} of 0.1 m rotating at 180 rotation per minute (rpm), is positioned on the simplified hull in the centerline amidship. Four different Apparent Wind Angles AWA equal to 30, 45, 60 and 90 degrees are simulated, as well as the three atmospheric boundary layers discussed above. The numerical setup is like the 2D and 3D empty domain simulations, with the following differences: the unsteady Reynolds-Averaged Navier-Stokes (uRANS) equations are solved with a temporal discretization scheme second-order accurate and a time-step t of 0.005 seconds to obtain a rotation of 5 degrees per time-step, with the simulations run for a total real time of 60 seconds. The domain has the same boundary conditions and dimensions as the 3D empty domain, with the zero of the coordinate system coinciding with the center bottom of the simplified hull and positioned 3.5L from the inlet and 4.5L from the outlet. More details about the hexahedral mesh can be found in Kontos et al. (2023).

3.2 Results

To assess the impact of the different atmospheric boundary layer stratifications on the performance of the Flettner rotor on a simplified hull, different coefficients are compared. The lift and drag coefficients, respectively perpendicular and parallel to the flow, and thrust and side force coefficients, related to the ship-coordinate system, are assessed. These coefficients are calculated as:

$$C_i = \frac{F_i}{0.5\rho S U_{rh}^2} \tag{6}$$

where the index i represents either lift, drag, thrust, or side force, ρ is the fluid density, S is the surface area of the rotor and endplate and U_{rh} is the speed at mid-height of the rotor. The mid-height of the rotor is equal to 35 meters for this case study and the corresponding velocity values are written in Table 1. Moreover, flow visualizations are showed to explain the results.

In Figure 5, the lift and drag coefficients for the Flettner rotor are presented. The drag and lift of a generic standalone rotor in uniform flow (Kontos et al. 2023) with the same spin ratio $SR = n\pi D/U_{rh}$, where n are rotations per second of the rotor, D is the rotor diameter and U_{rh} is the speed at mid-height of the rotor, are added to the plots in dash-dotted lines to try to estimate the effect of the hull on the performance of the rotor. The rotor in the unstable ABL has a SR equal to 4.5, for the neutral case the SR decreases to 4.1 and it has the lowest value of 3.4 for the stable stratification.

The drag and lift of the rotor on the simplified hull are always lower than for the generic standalone rotor. For each ABL, the values of the drag coefficient are relatively constant, except when AWA is equal to 90 degrees, where the drag increases for all three ABLs. A possible reason for the drag being visibly lower in the cases with an ABL with respect to the standalone rotor in uniform flow, can be the modified turbulence quantities: inlet profiles for turbulence kinetic energy k and specific turbulence dissipation rate ω and the values for C_μ and maximum μ_t/μ ratio. The lift decreases almost linearly for increasing AWAs. The case with stable ABL and AWA equal to 90 degrees behaves differently from the other points. It appears that the lift reaches a plateau at AWA of 60 degrees and becomes constant. The behavior of the lift decreasing with increasing AWA can be

explained when looking at Figs. 6-7. In Figure 6 the pressure distribution on the rotor, for the neutral ABL, is showed via the pressure coefficient C_p:

$$C_p = \frac{\Delta p}{0.5\rho U_{rh}^2} \tag{7}$$

with Δp the differential pressure, ρ the fluid density and U_{rh} the speed at mid-height of the rotor.

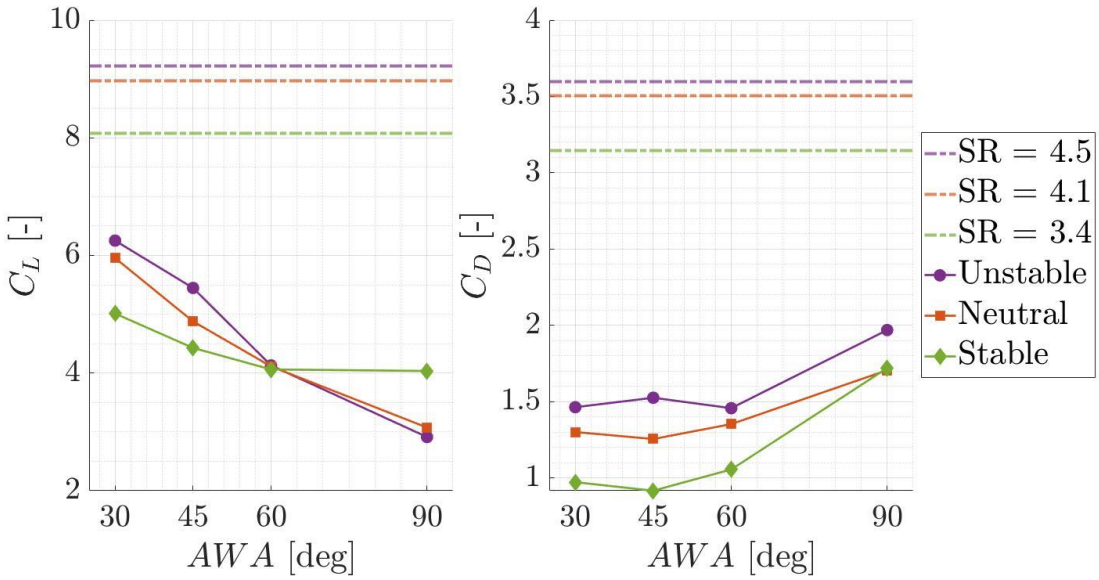

Figure 5. Lift coefficient C_L (left) and drag coefficient C_D (right) of the Flettner rotor for the three ABL and the four wind angles. The dash-dotted lines show the lift and drag coefficients for a generic standalone rotor in uniform flow (Kontos et al. 2023) with the same spin ratio SR of the rotor for the three ABL.

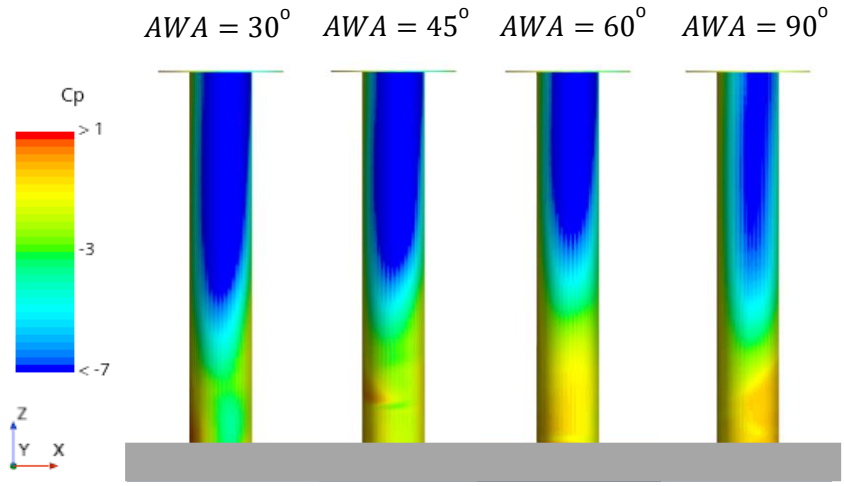

Figure 6. Pressure coefficient C_p distribution for the neutral ABL and the four different wind angles AWA.

With increasing AWA the area that generates lift decreases visibly (under-pressure area in dark blue). This effect is caused by the different incidence angles of the flow on the hull. The higher the AWA, the greater the incidence of the flow on the side and deck of the ship, causing a bigger recirculation bubble at the base of the rotor, as visible in Fig. 7.

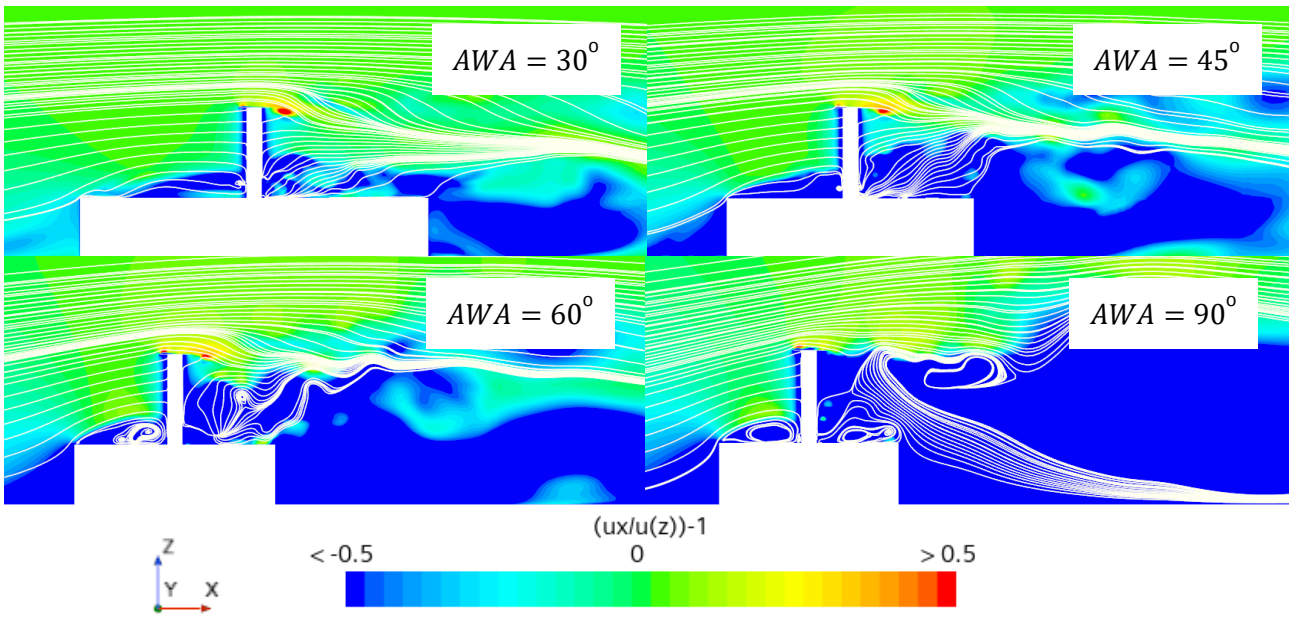

Figure 7. Normalized velocity in x-direction and streamlines for the neutral ABL and the four different wind angles AWA.

Figure 7 shows the velocity in x-direction normalized by the far filed ABL profile $u(z)$, centred in zero, meaning that areas with values lower than zero, represent areas where the flow decelerates, while areas with positive values show an acceleration of the flow. From this visualization, it is also possible to notice how the flow needs to travel a longer distance on the ship deck before encountering the Flettner rotor for smaller AWAs. Hence, additionally to the flow incidence angle, the length covered by the fluid on the hull affects the performance of the rotor as well.

From a ship performance point of view, the thrust and side force coefficients and their ratio are evaluated in Figure 8.

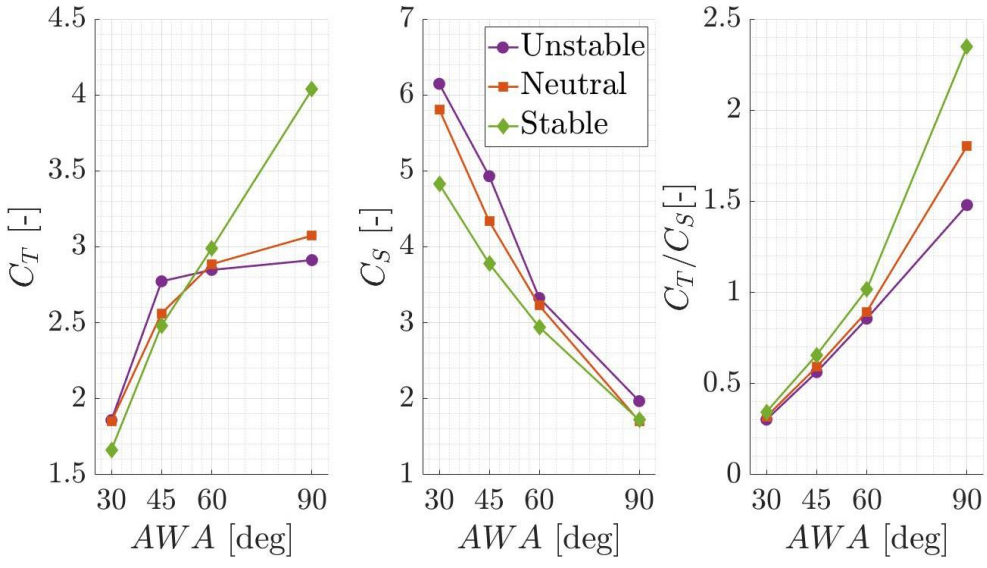

7

Figure 8. Thrust coefficient C_T (left), side force coefficient C_S (center) and their ratio C_T/C_S (right) for the Flettner rotor in the three ABL and the four wind angles.

The thrust and side force coefficients behave as expected, with a lower thrust and higher side force for lower wind angles. It is interesting to notice how the thrust coefficients for the unstable and neutral ABL hit a plateau from an AWA of 45 degrees, particularly for the unstable case, while for the stable stratification the thrust coefficient has an almost linear growth. Quasilinear is also the decay of the side force coefficient for all the stratifications. Note that the reference wind speed U_{rh} used in the normalization of the coefficients differs largely between the three stratifications (refer to Table 1), hence, even if in Fig. 8 the thrust and side force coefficients are similar between the three ABLs, the actual thrust and side force values differ. When looking at the ratio of the two coefficients C_T/C_S, it is noticeable the limited difference between the three ABL for the wind angles of 30, 45 and 60 degrees. Instead, for the AWA value of 90 degrees, the difference is more pronounced. This effect is probably caused by the characteristics of the flow which might not be well captured by the uRANS – two turbulence equations modelling used.

4. CONCLUSIONS

The influence of an unstable, neutral, and stable ABL on the force prediction of a Flettner rotor on a hull is studied. Firstly, 2D and 3D simulations with an empty domain are run to investigate the ABL correct description for the three stratifications. This investigation showed that the profiles are well-preserved throughout the domain, but more attention should be given to the area close to the bottom of the domain. It is also suggested to use an empty 3D domain to setup the ABL.

The simulations with the simplified hull equipped with a Flettner rotor, for the three different ABL stratifications, unstable, neutral, and stable, and for four different wind angles, equal to 30, 45, 60 and 90 degrees, showed several interesting aspects. For all three stratifications, the lift and drag coefficients are lower than for the case of a generic standalone rotor in uniform flow with the same spin ratio. The lower values for drag might be caused by the addition of turbulence quantities profiles at the inlet, and modification of two turbulence constants, needed to correctly describe the ABL profiles. From this study is also visible how the lift coefficient depends on the wind angle. For lower values of AWA, the incidence angle of the flow is less pronounced, causing for a smaller recirculation bubble to form on the deck of the ship. Moreover, the lower is the apparent wind angle, the longer is the distance that the fluid must travel on the deck. This length might allow the flow to have better characteristics before encountering the rotor. Looking at the ship performance, the behavior of the side force coefficient is quasi-linear, it decreases with increasing AWA. For what concerns the thrust coefficient instead, the stable ABL has a linear behavior, with thrust increasing for increasing AWA. In the case of the neutral and unstable stratifications, a plateau is reached at an AWA of 45 degrees; this behavior is more accentuated for the unstable ABL. The thrust and side force coefficients ratio is similar between the different ABL profiles for all the AWA values, except for the apparent wind angle equal to 90 degrees. This difference might be caused by the complex characteristics of the flow.

This study shows that the performance of a Flettner rotor is impacted by different ABL stratifications, and it is important to better understand and separate the mixed effects connected to the presence of the hull and the ABL profile, as well as investigate the large flow separation and recirculation present for apparent wind angles equal to 90 degrees, known to be challenging for RANS simulations.

5. ACKNOWLEDGEMENTS

The authors acknowledge the financial support from the European Commission and its agency CINEA, grant 101096673 and the Swedish Transport Agency, grant TRV 2022/30706. Additionally, the computations and data handling were enabled by resources provided by the National Academic Infrastructure for Supercomputing in Sweden (NAISS) at the PDC Center for High Performance Computing, KTH Royal Institute of Technology, partially funded by the Swedish Research Council through grant agreement no. 2022-06725.

6. REFERENCES

Bataille, J., Blayo, C. and Sergent P. (2023). PERFO: Methodology benchmark for Wind Assisted Propulsion Ship Performance Estimation. Proceedings of INNOV'SAIL 2023, Lorient, France.

Dhomé, U., Kuttenkeuler, J. and Segalini, A. (2023), Observation of the atmospheric boundary layer over the Atlantic and its effects for wind propulsion, under review, submitted to the *Journal of Ocean Engineering and Science*.

Garenaux, M., Schot, J. J. A. and Eggers R. (2020), Numerical Analysis of Flettner Rotors Performances on the MARIN Hybrid Transition Coaster, Proceedings of Hiper'20, Cortona, Italy.

Garenaux, M. and Schot, J. J. A. (2021). Flettner Rotors Performance and Interaction Effects on the MARIN Hybrid Transition Coaster. Proceedings of the International Conference on Wind Propulsion, London, UK.

ITTC 2022, Preparation, Conduct and Analysis of Speed/Power Trial, https://www.ittc.info/media/10174/75-04-01-011-2022.pdf.

Japan, A.I.O. (2007), Guidebook for CFD Predictions of Urban Wind Environment, Architectural Institute of Japan: Tokyo, Japan.

Kaltschmitt, M., Streicher, W. and Wiese, A. (2007), Renewable Energy. Technology, Economics and Environment, Springer, Berlin, Heidelberg.

Kim, J. W., Jang, H., Xu, W., Shen, Z., Kara, M., Yeon, S. and Yan, H. (2018), Numerical Modeling of Neutrally-Stable and Sustainable Atmospheric Boundary Layer for the Wind Load Estimation on an Offshore Platform, *Proceedings of the ASME 2018 37th International Conference on Ocean, Offshore and Arctic Engineering (OMAE),* 17-22 June, 2018, Madrid, Spain.

Kontos, S., Li, D.-Q., Wielgosz, C., Marimon Givannetti, L., Gerhardt, F., Werner, S. and Paakkari, V. (2023), Comparison of full-scale Flettner rotor performance prediction methods with sea trial data, *15th Symposium on High-Performance Marine Vehicles HIPER'23,* 18-20 September, 2023, Bernried, Germany.

Menter, F. R. (1994), Two-Equation Eddy_Viscosity Turbulence Models for Engineering Applications, *AIAA Journal,* vol. 32, no.8, pp. 1598-1605.

RahnamayBahambary, K., and Fleck, B. A. (2022), Effects of Inflow Parameters and Disk Thickness on an Actuator Disk inside the Neutral Atmospheric Boundary Layer, *Wind,* vol. 2, pp. 733-746.

Richards, P. J. and Hoxey, R. P. (1993), Appropriate boundary conditions for computational wind engineering models using the k-ε turbulence model, *J. Wind Eng. Ind. Aerodyn,* vol. 46-47, pp. 145-153.

Richards, P. J. and Norris, S. E. (2011), Appropriate boundary conditions for computational wind engineering models revised, *J. Wind Eng. Ind. Aerodyn.,* vol. 99, pp. 257-266.

Tian, L., Zhao, N., Wang, T., Zhu, W. and Shen, W. (2018), Assessment of Inflow Boundary Conditions for RANS Simulations of Neutral ABL and Wind Turbine Wake, *Journal of Wind Engineering & Industrial Aerodynamics,* vol. 179, pp. 215-228.

Tian, L., Song, Y., Zhao, N., Shen, W. and Zhu, C. (2020), Effects of Turbulence Modelling in AD/RANS Simulations of Single Wind & Tidal Turbine Wakes and Double Wake Interactions, *Energy*, v. 208, no. 118440.

Viola, I. M., Sacher, M., Xu, J. and Wang, F. (2015). A Numerical Method for the Design of Ships with Wind-Assisted Propulsion, *Ocean Engineering*, vol. 105, pp. 33-42.